

Effect of spin glass frustration on exchange bias in NiMn/CoFeB bilayers.

Sagarika Nayak,¹ Palash Kumar Manna,¹ Braj Bhusan Singh,¹ and Subhankar Bedanta^{1, a)}
*Laboratory for Nanomagnetism and Magnetic Materials (LNMM), School of Physical Sciences,
 National Institute of Science Education and Research (NISER), HBNI, P.O.- Jatni, 752050,
 India*

(Dated: October 2020)

Exchange bias in ferromagnetic/antiferromagnetic systems can be explained in terms of various interfacial phenomena. Among these spin glass frustration can affect the magnetic properties in exchange bias systems. Here we have studied a NiMn/CoFeB exchange bias system in which spin glass frustration seems to play a crucial role. In order to account the effect of spin glass frustration on magnetic properties, we have performed the temperature and cooling field dependence of exchange bias. We have observed the decrease of exchange bias field (H_{EB}) with cooling field (H_{FC}) whereas there is not significant effect on coercive field (H_C). Exponential decay of H_{EB} and H_C is found in these exchange bias systems. Further, training effect measurements have been performed to study the spin relaxation mechanism. We have fitted the training effect data with frozen and rotatable spin relaxation model. We have investigated the ratio of relaxation rate of interfacial rotatable and frozen spins in this study. The training effect data are also fitted with various other models. Further, we observed the shifting of peak temperature towards higher temperature with frequency from the ac susceptibility data.

I. INTRODUCTION

Historically, exchange bias was first studied in ferromagnetic (FM)/antiferromagnetic (AFM) systems^{1–5}. However, study of exchange bias in FM/spin-glass (SG) systems present a unique opportunity to explore how the SG component can also induce a unidirectional anisotropy leading to exchange bias. Exchange bias effects have been investigated in spin-glass AgMn, CuMn dilute alloys and also in FM/SG nanocomposite systems^{6,7}.

Mn based AFM materials like FeMn, IrMn, PtMn, PdMn, NiMn have a good thermal stability that is the main requirement of exchange biased spintronic devices⁸. One other important property of these above AFM's is their high Néel temperature T_N . For example, the T_N of $Ni_{50}Mn_{50}$ is 1070 K⁹. As-grown NiMn is paramagnetic with a face centred cubic (FCC) structure whereas post deposition annealing develops antiferromagnetic phase with face centred tetragonal (FCT) structure^{10,11}. The lattice constants of FCT NiMn are $a = b = 3.74 \text{ \AA}$ and $c = 3.52 \text{ \AA}$ ^{10,11}. EB properties was reported in Co/NiMn system deposited on Cu (001) substrate. EB has also been investigated in some of the AFM's such as NiMn, IrMn, Cr_2O_3 grown on Pt buffer layer¹¹. One can tune the microstructure by selecting the proper seed layer and hence the magnetic properties¹⁰. Exchange anisotropy at the FM/AFM interface can be controlled through proper selection of substrate, buffer layer and growth conditions due to the modification of structural orientations^{11–13}. AFM order can also be induced by choosing proper seed layer.

In this study, we have performed the temperature and cooling field dependence of exchange bias to investigate

the effect of interface and the SG 'bulk' on magnetic properties. Contribution of 'bulk' spins of NiMn has also been investigated from the variation of exchange bias field with its thickness. Besides, the increase in the relaxation rate ratio of rotatable and frozen spins indicates that not only the interface but also 'bulk' spins of NiMn contribute to the observed results.

II. EXPERIMENTAL DETAILS:

Deposition of $Ni_{50}Mn_{50}$ ($t = 5, 15 \text{ nm}$)/ $Co_{40}Fe_{40}B_{20}$ (5 nm) bilayers on Si (100) substrate has been performed by dc magnetron sputtering at room temperature (RT). Pt has been deposited on top of Ta as seed layer. Ta has also been deposited as capping layer to avoid oxidation. We have not performed post deposition annealing to induce AFM order in NiMn. However, Pt and Ta are deposited to promote AFM order¹¹ and modify interfacial exchange coupling through microstructure adjustment. The substrate was rotated at 20 rotation per minute (rpm) speed during deposition of all the magnetic layers to avoid growth induced uniaxial magnetic anisotropy. The rate of deposition of Ta, Pt, NiMn, and CoFeB are 0.13, 0.3, 0.14, and 0.16 $\text{\AA}/\text{sec}$, respectively. The magnetic measurements have been performed using a Quantum Design SQUID magnetometer (MPMS 3). All the sample details are given in table 1.

III. RESULTS AND DISCUSSION:

A. Magnetization vs temperature

To elucidate the magnetic nature of the films dc-magnetization measurements were performed as a function of temperature and fields. Figure 1 (a),(b) represent

^{a)} Electronic mail: sbedanta@niser.ac.in

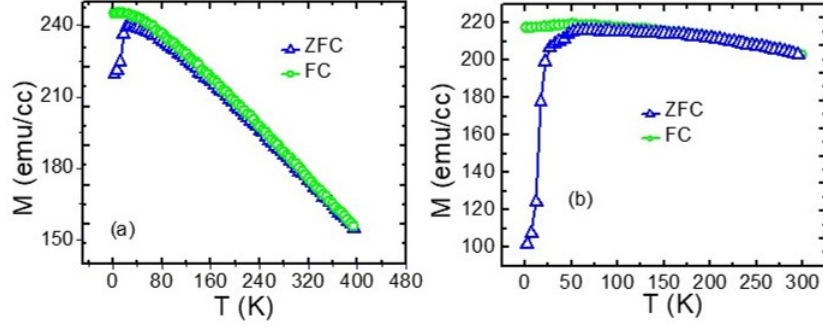


FIG. 1. (a)-(b) M vs T curves under ZFC, FC condition and $-d(M_{FC}-M_{ZFC})/dT$ vs T plots for the samples S1 and S2.

TABLE I. Details of sample nomenclature and configuration.

Sample name	Sample structure
S1	Si(100)/Ta(3 nm)/Pt(2.5 nm)/NiMn (5 nm)/CoFeB(5 nm)/Ta (3 nm)
S2	Si(100)/Ta(3 nm)/Pt(2.5 nm)/NiMn (15 nm)/CoFeB(5 nm)/Ta (3 nm)

the magnetization (M) vs temperature (T) curves under zero field cooled (ZFC) and field cooled (FC) conditions in a magnetic field of 10 mT. We found the peak temperatures (T_P) of 22, and 47 K in samples S1 and S2, thus, T_P increases with the thickness of NiMn. The T_P has broadened for higher thicknesses of NiMn due to increase in particle size and broader size distribution¹⁴. We found the bifurcation in ZFC and FC $M - T$ curves in all the samples at a temperature known as irreversibility temperature (T_{irr}).

B. Magnetic hysteresis

Figure 2 shows the magnetic hysteresis loops of sample S2 in zero field cooled (ZFC), positive and negative field cooled conditions (200 mT field), respectively at 10 K temperature. We found the negative exchange bias of 12.78 mT strength in ZFC condition indicating that the presence of positive exchange interaction at the interface. We found the negative and positive exchange bias in this sample under positive and negative field cooled conditions. This indicates the presence of positive and negative exchange interaction at the interface. However, the magnitude of exchange bias is different for field cooling in 200 mT (14.66 mT) and -200 mT (8.29 mT) fields, respectively. This, indicates that the coupling strength is different under positive and negative field cooling conditions, respectively.

C. Temperature dependence of exchange bias

It is reported in the literature that the temperature dependency behaviour of exchange bias and coercivity in FM/AFM and FM/SG systems is different^{15,16}. Our motivation is to investigate the temperature dependency

of EB in CoFeB/NiMn films and find out if it follows a trend similar to the FM/SG systems. The same experiments will also help us to find the blocking temperature of exchange bias. To perform temperature dependency of exchange bias, $M - H$ loops have been taken after FC from 400 K down to the desired temperatures (2, 10, 20, 30, 50, 100 and 300 K) in presence of 200 mT field. Figure 3 shows the plots of H_{EB} and H_C with temperature for all the samples and the experimental data were fitted using single exponential decay functions, given in eqs. (1) and (2), respectively, to find the presence of magnetic frustration in these systems^{15,17,18}.

$$H_{EB}(T) = H_{EB}^0 \exp(-T/T_1) \quad (1)$$

$$H_C(T) = H_C^0 \exp(-T/T_2) \quad (2)$$

where H_{EB}^0 and H_C^0 are the exchange bias and coercive fields at 0 K, T_1 and T_2 are the constants. Table 2 shows the parameters obtained from the fit of the H_{EB} , H_C vs T experimental data using eqs. (1) and (2), respectively.

It is reported in literature that the competition between Rudermann-Kittel-Kosuya-Yosida (RKKY) and direct exchange interactions gives the exponential decay of H_{EB} and H_C with temperature¹⁵. RKKY interaction is the coupling of internal spins of SG and FM spins whereas direct exchange interaction is the coupling of surface spins of SG and FM spins¹⁵. Thus, magnetic frustration gives exponential decay of H_{EB} and H_C with temperature.

We found T_g where the sudden rise of exchange bias occurs of ~ 50 K for all the samples. The increase in number of frozen spins at low temperature region (< 50 K) gives sudden rise in H_{EB} ¹⁹⁻²². But, we also observed a sudden rise of H_C at low temperature region (< 50 K). Thus, at low temperature, the presence of large number of low anisotropy rotatable spins give a sudden rise in

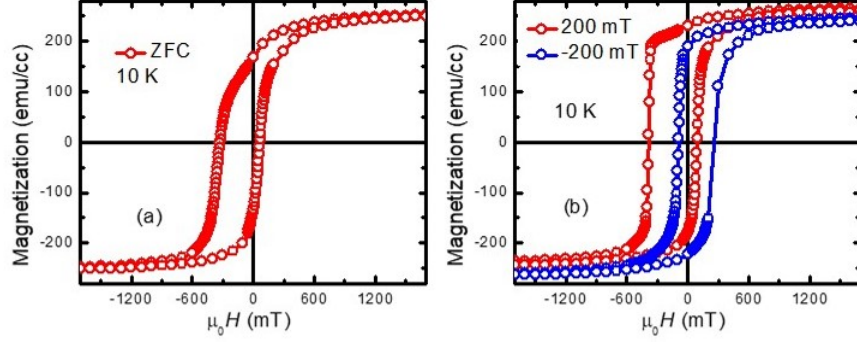


FIG. 2. Plots of hysteresis loop of sample S2 for negative, positive field cooling (FC) in 2 kOe field (b) and zero field cooling (ZFC) (a) states, respectively.

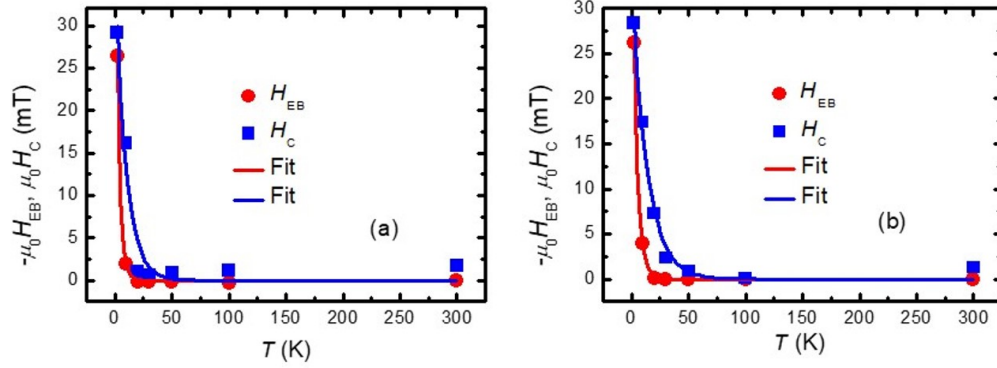


FIG. 3. (a)-(b) Plots of H_{EB} , H_C vs T experimental data along with their fits using eqs. (1) and (2) for samples S1 and S2, respectively.

H_C ¹⁹. The spin glass like frustration might be a reason for the presence of both frozen and low anisotropy rotatable spins at temperature below 50 K¹⁹. It is reported in literature that simultaneous decay of exchange bias field and coercive field w.r.t. temperature is not found in FM/AFM system¹⁶. The temperature where exchange bias vanishes is known as blocking temperature T_B . We found that T_B remains similar in all the sample.

D. Cooling field dependence of exchange bias

In order to find additional evidence for the nature of interface, cooling field dependence of exchange bias can be performed. Figure 4 shows the trends of H_{EB} and H_C with H_{FC} for the samples S1 and S2. To perform the cooling field dependency of EB, the samples were field cooled from 400 to 2 K in presence of various magnetic fields (0.05, 0.1, 0.2, 0.5, 1, 2, 3 and 5 T) and then $M - H$ loops were taken. In our study, we found the decrease of H_{EB} with increase in cooling field whereas H_C remains almost constant. Similar trend of H_{EB} and H_C with cooling field has been reported in FM/SG system²³. However, in a FM/AFM system, H_{EB} rises with increase in cooling field due to the enhancement in num-

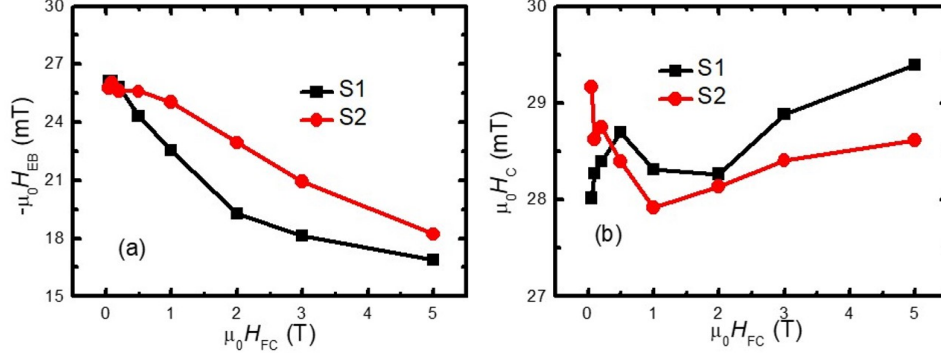
ber of pinned moments along the cooling field direction²⁴. We can interpret this behaviour as the presence of FM and AFM mix interactions in our systems. We found highest H_{EB} in sample S2 at 10 K temperature. Thus, H_{EB} is dependent on NiMn thickness indicating that not only the interface but also the ‘bulk’ part of the NiMn contribute to exchange bias.

E. Training effect

One of the important properties of the exchange bias systems is the training effect. Due to field cooling, the interfacial spins go to metastable states. However, consecutive cycling of the hysteresis loop without field cooling leads to relaxation of the metastable spins. The relaxation mechanism can be described by the training effect data analysis through various models. We field cooled (FC) the samples down to 5 K from 400 K in the presence of 500 Oe field to record the first hysteresis loop and then the consecutive loops were taken for training effect measurements. Figure 5 (a),(c) show the 1st, 2nd and 6th hysteresis loops and (d),(f) show the H_{EB} vs n data along with the fits using eqs. (4) and (5). The insets in figures 5 (d),(f) are the H_{EB} vs $n^{-1/2}$ data with linear

TABLE II. Fitting parameters obtained from the fits using eqs. (1) and (2), respectively.

Sample name	H_{EB}^0 (mT)	T_1 (K)	H_C^0 (mT)	T_2 (K)
S1	51.18 ± 1.56	3.02 ± 0.13	36.91 ± 3.68	9.57 ± 1.70
S2	42.22 ± 0.50	4.16 ± 0.08	33.49 ± 1.41	13.52 ± 1.02

FIG. 4. (a) H_{EB} (b) H_C vs H_{FC} plots for the samples S1 and S2.

fits. We found large decrease in H_{EB} in 2nd subsequent $M - H$ loop whereas gradual decrease is found after this ($n > 2$). We could not fit the H_{EB} vs n data using thermal relaxation model as it excludes $n = 1$ ²⁵. However, to determine the value of $H_{EB\infty}$, we have fitted the H_{EB} vs $n^{-1/2}$ data using the below equation²⁶;

$$H_{EB}(n) = H_{EB\infty} + \frac{k}{n^{1/2}} \quad (3)$$

where $H_{EB}(n)$ is the exchange bias field of n^{th} loop, $H_{EB\infty}$ is the exchange bias field in the limit of infinite number of loops ($n \rightarrow \infty$) and k is the system dependent constant. The values of $H_{EB\infty}$ obtained from eq. (3) are given in table 3. We found that $H_{EB\infty}$ and H_{EB} follow the similar trend. Power law decay of exchange bias has been observed in FM/AFM interfaces²⁵⁻²⁷. But, in this study, spin glass like frustration is present. Therefore, sudden decrease in H_{EB} is found in $n = 2$ loop due to less stability of interface spins under field reversal.

As eq. (3) failed to explain the training effect data, We considered the model given by Binek which is known as spin configurational relaxation model and is given below²⁸;

$$H_{EB}(n+1) - H_{EB}(n) = -\gamma_H(H_{EB}(n) - H_{EB\infty})^3 \quad (4)$$

where $H_{EB}(n)$, $H_{EB}(n+1)$ and $H_{EB\infty}$ are the exchange bias fields of the n^{th} , $(n+1)^{th}$ and in the limit of infinite number of loops, respectively. γ_H is the characteristic decay rate of the training effect and defined as $\gamma_H = b/(K^2\zeta)$ where K is a constant proportional to the exchange coupling strength in FM/AFM system, ζ is the inverse of relaxation time and b is another constant²⁵. The small value of γ_H indicates large deviation

from equilibrium steady state and hence large training effect which is according to relaxation theory²⁹. Such spin configurational relaxation in training effect data is also reported for a FM-SG interface.

Another approach to explain training effect data was given by Mishra et al. which considers relaxation rate of both the rotatable and frozen spins at the interface and is described below³⁰;

$$H_{EB}(n) = H_{EB\infty} + A_f \exp(-n/P_f) + A_i \exp(-n/P_i) \quad (5)$$

where A_f , P_f are the interfacial frozen spin parameters and A_i , P_i are the interfacial rotatable spin parameters of the NiMn/CoFeB system. P_f and P_i are the relaxation rates of interfacial frozen and rotatable spins, respectively. P_f and P_i are dimensionless. A_f and A_i have the dimension of mT. We observed that A_f and A_i are decreasing with the thickness of NiMn. Thus, the frozen and rotatable interfacial spin components become lesser with increase in thickness of NiMn. Also, A_f is higher than A_i indicating that the frozen spin components have major contribution to the training effect. P_f is almost constant for all the samples. However, P_i increases as NiMn becomes thicker leading to an increment in P_i/P_f indicating that not only the interface but also 'bulk' of NiMn contributes to the relaxation.

The model given by Binek considers only instability of interface AFM magnetization whereas Mishra et al. introduced the relaxation of frozen and rotatable interface spins. Parameters obtained by the fits using eqs. (3), (4) and (5) are given in table 3. In the training effect $M - H$ loops (figure 5), the magnitude of H_{EB} reduces in the descending part of the loop whereas the magnitude remains constant in the ascending part of the loop similar to FM/AFM systems³¹.

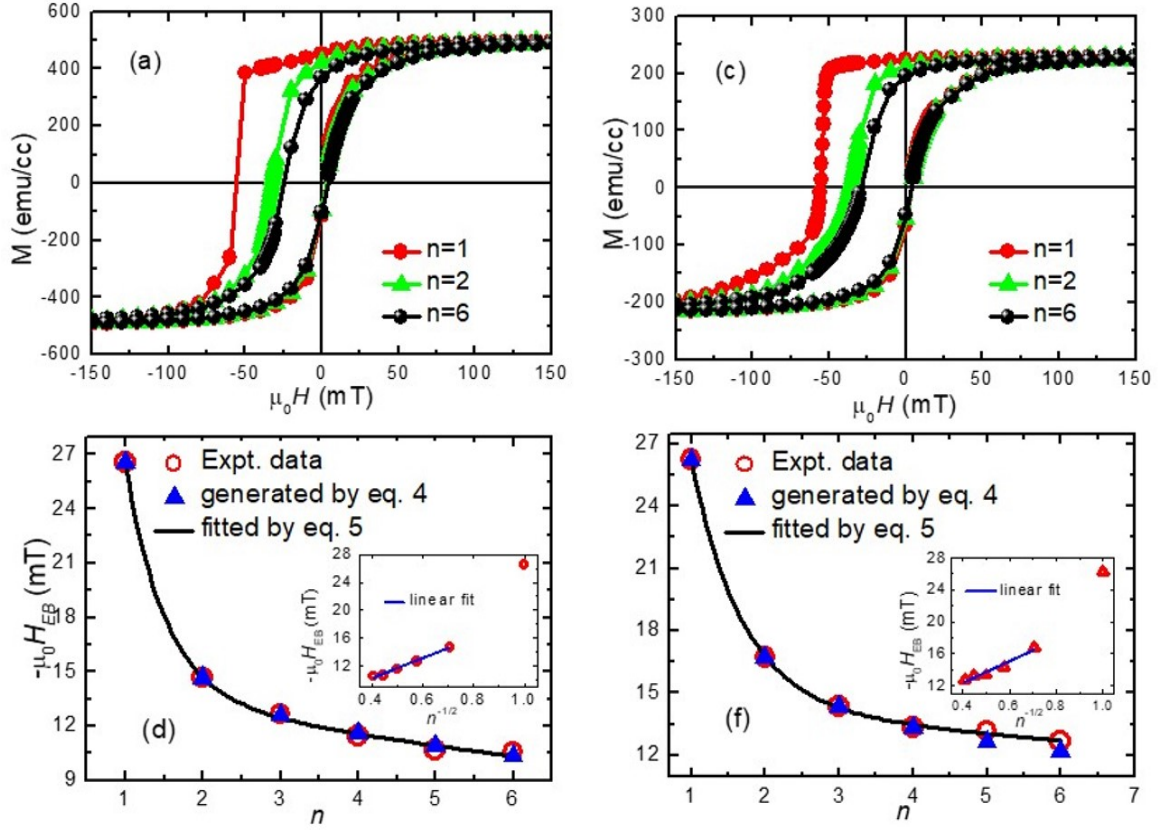


FIG. 5. (a),(c) 1^{st} , 2^{nd} , and 6^{th} subsequent hysteresis loops of samples S1 and S2. (d),(f) solid circles are the experimental H_{EB} vs n data, blue triangular data points are generated from eq. (4) and solid line is the fitted data using eq. (5). The insets of the plots (d),(f) show the experimental H_{EB} vs $n^{-1/2}$ data along with the fits using eq. (3) for the samples S1 and S2.

TABLE III. The fitting parameters obtained using eqs. (3), (4) and (5).

Sample name	$H_{EB\infty}$ (mT)	γ_H (10^{-3} mT^{-2})	A_f (mT)	A_i (mT)	P_f	P_i	P_i/P_f
S1	4.42 ± 0.49	1.88	93.48 ± 3.13	10.27 ± 0.48	0.50 ± 0.08	10.88 ± 1.36	21.76
S2	6.98 ± 0.83	2.55	51.61 ± 4.55	7.85 ± 0.68	0.67 ± 0.05	19.05 ± 6.19	28.43

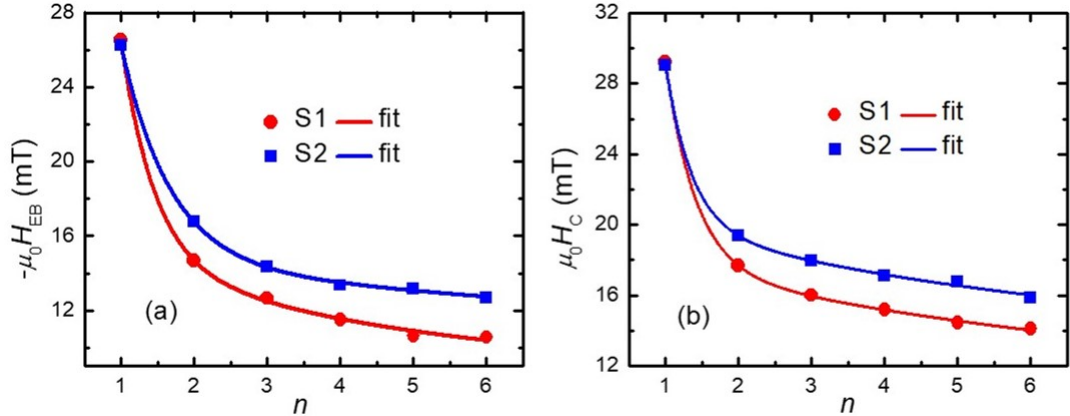


FIG. 6. Solid symbols are the experimental data of (a) H_{EB} and (b) H_C vs n for all the samples with the solid lines are the fits using eq. (6) for the samples S1 and S2.

Above models describe the training induced relaxation of interface magnetization. However, we want to con-

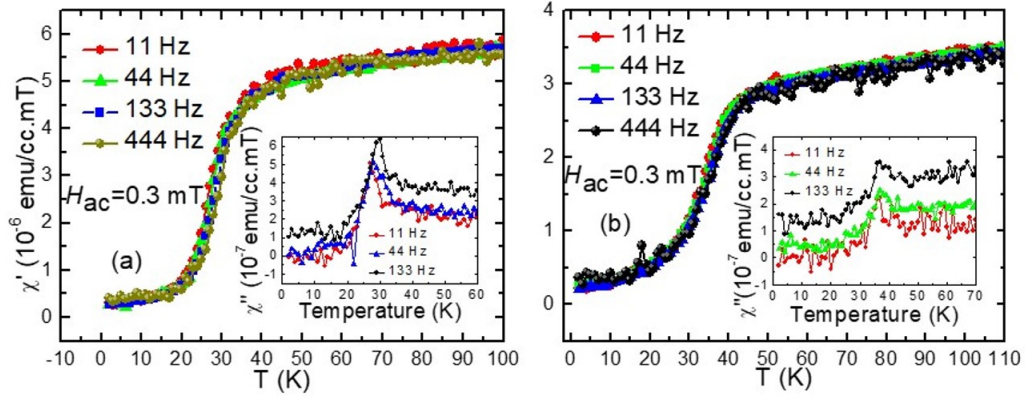


FIG. 7. (a),(b) Plots of real part of ac susceptibility (χ') vs temperature (T) and insets show the imaginary part of ac susceptibility (χ'') vs temperature (T) plot at different frequencies for the samples S1 and S2.

TABLE IV. The fitting parameters obtained utilizing eq. (6).

Sample name	$H_E(\infty)$ (mT)	A_s^{EB} (mT)	A_i^{EB} (mT)	n_0^{EB}	τ_s^{EB}	τ_i^{EB}	$H_C(\infty)$ (mT)	A_s^{CO} (mT)	A_i^{CO} (mT)	n_0^{CO}	τ_s^{CO}	τ_i^{CO}
S1	8.52 ± 0.21	12.31 ± 1.05	6.13 ± 0.21	0.98 ± 0.20	0.45 ± 0.09	4.57 ± 0.98	10.21 ± 0.09	12.11 ± 0.09	7.35 ± 0.35	0.98 ± 0.06	0.41 ± 0.03	7.65 ± 0.75
S2	8.71 ± 0.05	11.76 ± 0.15	5.78 ± 0.09	1.00 ± 0.03	0.67 ± 0.06	13.57 ± 1.12	12.86 ± 0.31	9.06 ± 0.15	6.89 ± 0.09	1.00 ± 0.08	0.36 ± 0.03	6.32 ± 0.22

firm that not only FM/SG interface but also ‘bulk’ spins of SG contribute to relaxation in training effect. In order to separate the contribution of the ‘bulk’ NiMn and interface spins of NiMn/CoFeB system towards training induced relaxation, we fitted the training effect data using the following eq.³²;

$$\begin{aligned} \pm H_{E,C}(n) = & \pm H_{E,C}(\infty) \\ & + A_s^{EB,CO} \exp[-(n - n_0^{EB,CO})/\tau_s^{EB,CO}] \\ & + A_i^{EB,CO} \exp[-(n - n_0^{EB,CO})/\tau_i^{EB,CO}] \end{aligned} \quad (6)$$

where $H_E(\infty)$ and $H_C(\infty)$ are the limiting values of exchange bias and coercive fields after infinite number of loop run ($n \rightarrow \infty$). $A_s^{EB,CO}$ and $A_i^{EB,CO}$ have the dimension of magnetic field in which the superscripts EB, CO correspond to the exchange bias and coercivity whereas the subscripts s, i indicate the weights of spin glass ‘bulk’ and spin-glass-like interface, respectively. n, n_0 and τ have the dimensions of time. Relaxation velocity is determined by τ and the relaxation will be faster for smaller τ . n_0 is the shifting coefficient. Figure 6 shows the H_{EB}, H_C vs n data for all the samples along with the fits using eq. (6). Table 4 shows the parameters obtained by the fits using eq. (6). The amplitude of decay A_i^{EB} for the spin-glass-like interface is found to be dependent on NiMn thickness whereas A_s^{EB} which is the amplitude of decay of ‘bulk’ NiMn spins is independent on the NiMn thickness. It is found that the magnitude of A_s^{EB} is higher than A_i^{EB} in all the samples. Similarly, the magnitude of A_s^{CO} is higher than A_i^{CO} . In all

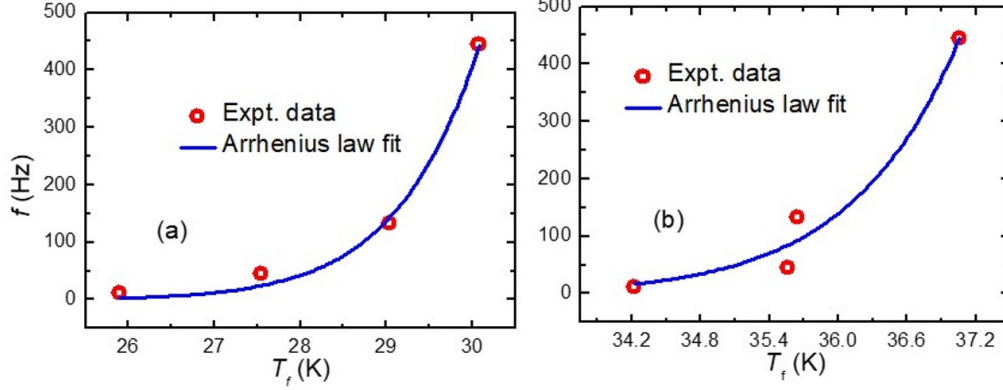
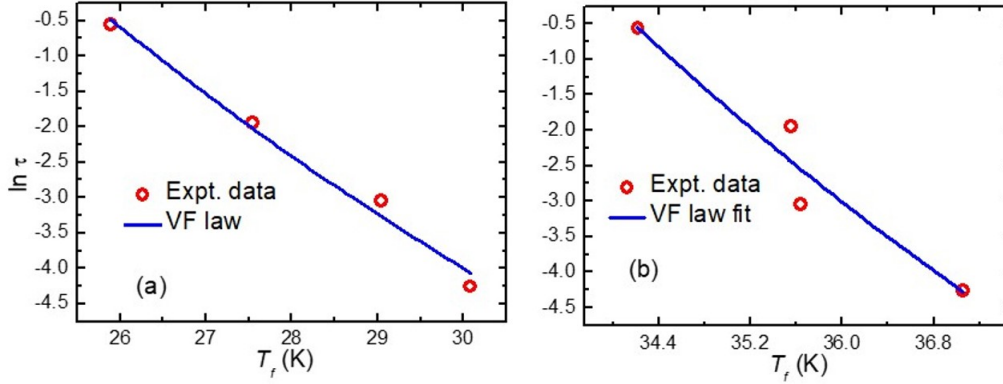
samples, τ_i^{EB} has a greater magnitude than τ_s^{EB} indicating that the ‘bulk’ spins of NiMn spin glass relax faster than spin-glass-like interface spins. Thus, for smaller n , ‘bulk’ NiMn spins play dominant role whereas the spin-glass-like interface spins play role for higher n in training induced relaxation. The relaxation rate of spin-glass-like interface spins τ_i^{EB} is dependent on the NiMn thickness. It is also reported that the value of shifting coefficient n_0 is approx. 1 in FM/SG system. We also found the value of $n_0 \sim 1$ in this study.

F. AC susceptibility

To provide additional evidence about the magnetic nature of NiMn in the NiMn/CoFeB bilayer, we performed ac susceptibility measurements w.r.t. temperature at different frequencies in presence of an ac field of 0.3 mT. Figure 7 shows the plots of real part of ac susceptibility (χ') vs temperature and the insets show the plots of imaginary part of ac susceptibility (χ'') vs temperature at different frequencies for all the samples. We found that the peak temperature T_f , obtained from the real part of the ac susceptibility (χ') vs temperature (T) plot, shifts towards higher temperature confirming the SG nature of NiMn. T_f has shifted from ~ 26 K at 11 Hz to ~ 30 K at 444 Hz in sample S1. In sample S2, T_f gets shifted from ~ 34 K at 11 Hz frequency to ~ 37 K at 444 Hz frequency. The dynamic behaviour of magnetic system is governed by temperature also³³. Neel-Arrhenius (N-A) proposed a model which considers both the anisotropy energy $E_a = K_{eff}V$ and thermal energy $k_B T$. K_{eff} is the

TABLE V. Fitting parameters obtained using eqs. (7) and (8) of all the samples.

Sample name	N-A Model		V-F law		
	f_0 (Hz)	E_a/k_B (K)	τ_0 (s)	E_{VF}/k_B (K)	T_{VF} (K)
S1	$2.44 \times 10^{16} \pm 7.22 \times 10^{14}$	951.88 ± 111.90	$4.66 \times 10^{-12} \pm 6.91 \times 10^{-13}$	657.73 ± 53.12	0.20 ± 0.10
S2	$5.88 \times 10^{19} \pm 4.22 \times 10^{18}$	1461.04 ± 2.92	$3.19 \times 10^{-12} \pm 3.26 \times 10^{-13}$	438.74 ± 83.32	17.29 ± 1.71

FIG. 8. (a),(b) Plots of frequency (f) vs T_f experimental data with fitted data using N-A model for the samples S1 and S2.FIG. 9. (a),(b) Plots of $\ln(\tau)$ vs T_f experimental data with fitted data using V-F law for the samples S1 and S2.

effective anisotropy constant which takes into account surface, interface anisotropies etc. and V is the volume of particles. N-A model can be expressed as follows³³;

$$f = f_0 \exp(-E_a/K_B T_f) \quad (7)$$

where, f is the rate of flipping of magnetization between the two lowest energy states, an attempt frequency is defined as f_0 whose value for superparamagnets lies between 10^8 to 10^{12} Hz^{34,35}. k_B is the Boltzmann constant. The values of f_0 are found to be larger than the usual values of the superparamagnets. We obtained unphysical large E_a/k_B values from the fit using N-A model³⁴. The plots of frequency (f) vs T_f are shown in figure 8. It is assumed that the presence of interactions tune T_f through the modification of energy barrier. Thus, the anisotropy energy E_a and relaxation time are tuned not only by thermal energy but also by the interaction present in the system³³. To explain magnetically interacting system,

Vogel-Fulcher (V-F) described a theory^{33,36,37};

$$\tau = \tau_0 \exp(E_{VF}/K_B(T_f - T_{VF})) \quad (8)$$

Where, E_{VF} is the activation energy and Vogel-Fulcher temperature, T_{VF} , is a measure of the interaction strength. The value of τ_0 for a spin glass or cluster spin glass system lies in-between 10^{-12} to 10^{-14} s³⁷. Figure 8 shows the fit of T_f vs $\ln\tau$. We found the values of τ_0 similar to spin glass systems. The fitting parameters obtained using eqs. (7) and (8) are given in table 5.

In summary, presence of magnetic frustration can be concluded from the exponential decay of both H_{EB} and H_C with temperature, the cooling field dependence of exchange bias, ac susceptibility measurements etc. We found the blocking temperature T_b , where maximum number of particles are unblocked, from the $M - T$ measurements. Sudden rise in H_{EB} is found below ~ 50 K from temperature dependence of exchange bias due to

the role of frozen spins of SG. Again, the decrease in exchange bias field H_{EB} is observed with the increase in cooling field H_{FC} . We fitted the training effect data using various models. Among them, thermal relaxation model fails to explain training effect. We have investigated from the training effect fitting that not only the interface but also ‘bulk’ NiMn spins contribute for the relaxation. The relaxation time τ_0 obtained from V-F law fitting indicates that the system has non-negligible interaction like spin glass.

CONFLICTS OF INTEREST

There are no conflicts to declare.

ACKNOWLEDGMENTS:

The authors thank Department of Atomic Energy (DAE) for providing the financial support. BBS acknowledges DST for INSPIRE faculty fellowship. We acknowledge Pushpendra Gupta for his help in SQUID measurements.

- ¹H. Xi, R. M. White, Z. Gao, and S. Mao *J. Appl. Phys.*, 2002, **92**, 4828.
- ²X. Chi, and Y. Hu *Nanotechnology*, 2020, **31**, 125703 (9pp).
- ³S. Zhang, and Z. Li *Phys. Rev. B*, 2001, **65**, 054406.
- ⁴X. W. Wu, and C. L. Chien *Phys. Rev. Lett.*, 1998, **81**, 2795.
- ⁵S. Zhong, D. Jun, and Z. Shi-Ming *Chin. Phys. B*, 2014, **23**, 027503.
- ⁶M. Ali, P. Adie, C. H. Marrows, D. Greig, B. J. Hickey, and R. L. Stamps *Nat. Mater.*, 2007, **6**, 70-75.
- ⁷F.-T. Yuan, J.-K. Lin, Y. D. Yao, and S.-F. Lee *Appl. Phys. Lett.*, 2010, **96**, 162502.
- ⁸B. Dai, J. W. Cai, W. Y. Lai *J. Magn. Magn. Mater.*, 2003, **257**, 190-194.
- ⁹V. Baltz, A. Manchon, M. Tsoi, T. Moriyama, T. Ono, Y. Tserkovnyak *Rev. Mod. Phys.*, 2018, **90**, 015005.
- ¹⁰S. Groudeva-Zotova, D. Elefant, R. Kaltoven, D. Tietjen, J. Thomas, V. Hoffmann, C.M. Schneider *J. Magn. Magn. Mater.*, 2003, **263**, 57-71.
- ¹¹A. Akbulut, S. Akbulut, F. Yildiz *J. Magn. Magn. Mater.*, 2016, **417**, 230-236.
- ¹²T. Lin, D. Mauri, N. Staud, C. Hwang, J. K. Howard, and G. L. Gorman *Appl. Phys. Lett.*, 1994, **65**, 1183.
- ¹³T. Yang and W. Y. Lai *J. Phys. D: Appl. Phys.*, 1999, **32**, 2856-2860.
- ¹⁴P. Anil Kumar, G. Singh, W. R. Glomm, D. Peddis, E. Wahlström⁵ and R. Mathieu *Mater. Res. Express*, 2014, **1**, 036103.
- ¹⁵C. Wang, L. Zhou, Q. Fu, Y. Tian, S. Wang, H. Gou, J. Ai, L. Zhang, and F. Xue *J. Magn. Magn. Mater.*, 2018, **449**, 372-377.
- ¹⁶M. Ali, C.H. Marrows, M. Al-Jawad, B.J. Hickey, A. Misra, U. Nowak, and K.D. Usadel, *Phys. Rev. B*, 2003, **68**, 214420.
- ¹⁷J. F. Ding, O. I. Lebedev, S. Turner, Y. F. Tian, W. J. Hu, J. W. Seo, C. Panagopoulos, W. Prellier, G. Van Tendeloo, and T. Wu *Phys. Rev. B*, 2013, **87**, 054428.
- ¹⁸L. Xie, H. L. Huang, and Y. L. Lu *AIP Adv.*, 2017, **7**, 015207.
- ¹⁹F. Spizzo, M. Tamisari, E. Bonfiglioli and L. Del Bianco *J. Phys.: Condens. Matter*, 2013, **25**, 386001 (7pp).
- ²⁰J. McCord, and S. Mangin *Phys. Rev. B*, 2013, **88** 014416.
- ²¹C. Zhu, Z. Tian, L. Wang, S. Yuan *J. Magn. Magn. Mater.*, 2015, **393** 116-120.
- ²²S. Chandra, H. Khurshid, W. Li, G. C. Hadjipanayis, M. H. Phan, and H. Srikanth *Phys. Rev B*, 2012, **86** 014426.
- ²³W. B. Rui, Y. Hu, A. Du, B. You, M. W. Xiao, W. Zhang, S. M. Zhou and J. Du *Sci. Rep.*, 2015, **5**, 13640.
- ²⁴L. Del Bianco, F. Spizzo, M. Tamisari, S. Laureti *Solid State Commun.*, 2011, **151**, 351-35.
- ²⁵P.V. Muhammed Shameem, M. Senthil Kumar *J. Magn. Magn. Mater.*, 2018, **458**, 241-252.
- ²⁶D. Paccard, C. Schlenker, O. Massenet, R. Montmory, and A. Yelon *Phys. Status Solidi B*, 1966, **16**, 301.
- ²⁷J. Barman, T. Bora, S. Ravi *J. Magn. Magn. Mater.*, 2015, **385**, 93-98.
- ²⁸C. Binek *Phys. Rev. B*, 2004, **70**, 014421.
- ²⁹L. G. Wang, C. M. Zhu, D. L. G. C. Bao, Z. M. Tian, S. L. Yuan *J Mater Sci*, 2015, **50**, 5904-5911.
- ³⁰S. K. Mishra, F. Radu, H. A. Dürr, and W. Eberhardt *Phys. Rev. Lett.*, 2009, **102** 177208.
- ³¹F.-T. Yuan, Y. D. Yao, S. F. Lee, and J. H. Hsu *J. Appl. Phys.*, 2011, **109**, 07E148.
- ³²X. Chi, W. Rui, J. Du, S. Zhou, A. Du, and Y. Hu *Appl. Phys. Lett.*, 2016, **108**, 172401.
- ³³Y. Slimani, A. Baykal, A. Manikandan *J. Magn. Magn. Mater.*, 2018, **458**, 204-212.
- ³⁴S. D. Tiwari, and K. P. Rajeev *Phys. Rev. B*, 2005, **72**, 104433.
- ³⁵A. Labarta, O. Iglesias, Ll. Balcells, and F. Badia *Phys. Rev. B*, 1993, **48**, 10240-10246.
- ³⁶S. Bedanta and W. Kleemann *J. Phys. D: Appl. Phys.*, 2009, **42**, 013001 (28pp).
- ³⁷K D. Chandrasekhar, A. K. Das and A. Venimadhav *J. Phys.: Condens. Matter*, 2012, **24**, 376003 (8pp).